Quantum Information and Computation, Vol. 15, No. 7&8 (2015) 0582–0600

QUANTUM STATE TRANSFER IN DISORDERED SPIN CHAINS: HOW MUCH ENGINEERING IS REASONABLE?

ANALIA ZWICK [1,2,3] GONZALO A. ÁLVAREZ [1,3] JOACHIM STOLZE [3] OMAR OSENDA [2]

[1] *Department of Chemical Physics, Weizmann Institute of Science, 76100 Rehovot, Israel*

[2] *Facultad de Matemática, Astronomía y Física and Instituto de Física Enrique Gaviola Universidad Nacional de Córdoba, 5000 Córdoba, Argentina*

[3] *Fakultät Physik, Technische Universität Dortmund, D-44221 Dortmund, Germany*

Received June 9, 2013
Revised November 3, 2014

The transmission of quantum states through spin chains is an important element in the implementation of quantum information technologies. Speed and fidelity of transfer are the main objectives which have to be achieved by the devices even in the presence of imperfections which are unavoidable in any manufacturing process. To reach these goals, several kinds of spin chains have been suggested, which differ in the degree of fine-tuning, or engineering, of the system parameters. In this work we present a systematic study of two important classes of such chains. In one class only the spin couplings at the ends of the chain have to be adjusted to a value different from the bulk coupling constant, while in the other class every coupling has to have a specific value. We demonstrate that configurations from the two different classes may perform similarly when subjected to the same kind of disorder in spite of the large difference in the engineering effort necessary to prepare the system. We identify the system features responsible for these similarities and we perform a detailed study of the transfer fidelity as a function of chain length and disorder strength, yielding empirical scaling laws for the fidelity which are similar for all kinds of chain and all disorder models. These results are helpful in identifying the optimal spin chain for a given quantum information transfer task. In particular, they help in judging whether it is worthwhile to engineer all couplings in the chain as compared to adjusting only the boundary couplings.

Keywords: quantum channels, spin dynamics, perfect state transfer, quantum information, decoherence, mesocopic echoes

Communicated by: S Braunstein & K Molmer

1 Introduction

Quantum information processing [1] relies on a number of key elements of technology. The qubits (quantum bits) as elementary units of quantum information are required to fulfill certain conditions [2]. The information contained in the qubits or registers of qubits must be processed by quantum gates. Since non-trivial quantum computers are likely to contain a large number of quantum gates and registers, information must be transferred between different elements of the computer. Quantum information is encoded in states of single separate qubits or in entangled states of several qubits. Transfer of single-qubit states over long distances can be achieved by photons. For the short distances between different elements of a quantum computer, however, photons do not provide the most practical means of quantum

state transfer. Instead, linear arrays of suitably coupled qubits appear to be more promising. Using the natural identification of a qubit with a spin-1/2 system, these arrays have come to be known as *quantum spin chains*. Many different spin chain models and quantum state transfer protocols have been studied from different points of view during the last few years [3, 4]. In the present study we want to focus on the state transfer in spin-1/2 XX chains with nearest-neighbor coupling in the presence of static coupling disorder. While XX chains under suitable circumstances can be used for the transfer of entangled multi-qubit states [5, 6], we restrict ourselves to single-qubit state transfer here.

Disorder can spoil quantum information transfer through spin chains in many different ways. External fields fluctuating in time and/or space may act on each spin separately, and the couplings connecting the spins may deviate from their design values or even fluctuate in time. In the present study all external fields are assumed to be strictly zero and all couplings are assumed to be time-independent. Also, no active control measures involving time-dependent fields or couplings will be considered. The kind of disorder studied here is assumed to arise from fabrication defects which are unavoidable in the process of building an artificial quantum spin chain for quantum state transfer. There are many coupling designs which yield perfect or near-perfect quantum state transfer under ideal circumstances, and it is important to assess the robustness of those designs against disorder.

The quality of transmission, that is, the similarity between the transmitted state at one end of the spin channel and the received state at the other end, is usually measured by the fidelity [7]. For a set of manufactured quantum spin chains, the best-case, worst-case, or average fidelities may be relevant, depending on the situation at hand. The situation we imagine is a future "integrated quantum circuit" with a large number of quantum gates and a correspondingly large number of spin chains connecting gates and registers. In that case the average fidelity will be most relevant, provided there are means to reroute the quantum information in order to circumvent "weak links", *i.e.* low-fidelity spin chains in the network. This point of view, focusing on the average fidelity, is common to many existing studies [8, 9, 10, 11, 12, 13]; see, however, Ref. [14] for a different point of view.

A disordered chain is represented by a spin-chain Hamiltonian where the exchange couplings become random variables that model the static disorder affecting the interaction between spins [8, 10, 15, 11, 12, 16]. Solving the Hamiltonian eigenvalue problem for many realizations of the disorder then leads, naturally, to an eigenvalue distribution and probability distributions for the eigenvectors. Both probability distributions, for the eigenvalues and eigenvectors, determine the behavior of the averaged fidelity [11], but are up to now poorly understood. Moreover, apparently the same scaling law for the decay of the averaged fidelity holds for a broad class of spin couplings and two different models of static disorder [12].

Many protocols for high-fidelity quantum information transmission have been developed [7, 5, 17, 18, 19, 20, 9, 10, 21, 22, 13, 23, 24]. In this work we focus on some of the main proposals based on the natural Hamiltonian dynamics of spin chains with time-independent nearest-neighbor couplings and without any external fields. These proposals can be grouped into two classes depending on the extent to which the spin couplings are being tuned, or *engineered*. The first class comprises chains in which the state transmitted is exactly equal to the state received [25, 26, 6, 27, 28], *i.e.* these systems provide *perfect state transfer* (PST). PST can only be achieved if all couplings between spins are properly adjusted, hence one might

also classify these systems as *fully engineered*. The second class of systems [29, 21, 30, 31, 32, 33, 34, 12, 35, 36, 37, 38] is characterized by a much smaller degree of engineering leading to very good (but not perfect) state transfer. These systems require only the adjustment of the boundary couplings of the chain, hence they may be called *boundary-controlled* chains. Note, however, that this term does not imply any active control of the system when in use: the boundary couplings are fixed once and for all in the manufacturing process. Since there is no unique prescription as to the "right" value of the boundary couplings, they may be optimized in different ways to meet different objectives; for example, there is a trade-off between fidelity and speed of transmission [11, 12]. In contrast to the PST systems we will call this class *optimizable state transfer* (OST) systems [a] In the presence of static disorder in the exchange couplings, OST systems were shown [12, 32, 39] to offer reliable and robust state transmission. In particular we showed [12] that the quality of information transfer in OST systems under perturbation by disorder can be comparable to or even better than that of fully engineered PST systems. In order to make the present study self-contained we review below some of that earlier work, focusing on the most robust systems. We illustrate the properties of the chains which ensure, on average, a successful state transmission. From these properties, it can be understood why seemingly different systems show qualitatively the same performance when subjected to the same kind of disorder. In our numerical studies it turns out that in all systems the transfer fidelity shows similar scaling laws with respect to the length of the chain and the strength of the disorder. Our results may help in identifying the optimal spin chain for a given quantum information transfer task. In particular, they help in deciding whether it is worthwhile to engineer all couplings in the chain as compared to adjusting only the boundary couplings.

The paper is organized as follows. In Section 2 we present the Hamiltonian of the quantum spin chains whose performance we want to compare, the transfer protocol and the disorder model. In Section 3.1 we analyse the properties related to eigenvalues and eigenvectors that result in a robust transfer of quantum states, building in part on our earlier work [11, 12]. In Section 4 we study in detail how fast and how reliably the different spin chains can transfer quantum information. In a previous study [8] it was found that the averaged fidelity $\overline{F}$ of a specific type of spin chain of length N depends on the scaling variable $N\varepsilon^\beta$, where ε is the strength of the disorder and $\beta = 2$. We find that other types of spin chains obey similar scaling laws. In Section 4 we furthermore compare the different systems and show how they can be grouped in several classes, before we conclude with Section 5.

2 Spin channels

We consider two different types of spin chains for state transfer: *boundary-controlled* optimizable state-transfer (OST) type [29, 31, 12, 30, 34], and *perfect state transfer* (PST) type [5, 25, 6, 26, 27, 40, 11]. Both are described by a XX Hamiltonian

$$H = \frac{1}{2}\sum_{i=1}^{N-1} J_i \left(\sigma_i^x \sigma_{i+1}^x + \sigma_i^y \sigma_{i+1}^y\right) \tag{1}$$

[a] The word "optimized" in place of "optimizable" used earlier [12] suggests a unique optimum which actually does not always exist.

where $\sigma_i^{x,y}$ are the Pauli matrices, N is the chain length, and J_i are the time-independent exchange interaction couplings between neighboring spins. The J_i are allowed to vary in space, but we assume mirror symmetry with respect to the center of the chain, $J_i = J_{N-i}$.

The boundary-controlled spin chains are a mono-parametric family of chains, such that

$$J_1 = J_{N-1} = \alpha J, \quad \text{and} \quad J_i = J, \ \forall i \neq 1, N-1. \tag{2}$$

The parameter α modifies the strength of the exchange interaction of the boundary spins i=1 and i=N with their respective nearest-neighbor spins, otherwise the chains are homogeneous.

In contrast, PST spin chains are designed to allow for perfect state transmission at some time. That calls for a certain structure of the energy spectrum, and by solving an inverse eigenvalue problem the corresponding values of the couplings J_i can be determined. We refer to these chains as *fully engineered* since all $N-1$ couplings J_i must be adjusted properly.

2.1 Protocol and fidelity of state transmission

The goal is to transmit a quantum state $|\psi_0\rangle$ initially stored on the first spin ($i = 1$) to the last spin of the chain ($i = N$). $|\psi_0\rangle$ is an arbitrary normalized superposition of the spin down ($|0\rangle$) and up ($|1\rangle$) states of the first spin, with the remaining spins of the chain initialized in a spin down state. The Hamiltonian (1) conserves the number of up spins because $[H, \Sigma_i \sigma_i^z] = 0$. Therefore the component of the initial state $|\mathbf{0}\rangle = |00...0\rangle$ is an eigenstate of H and only the component $|\mathbf{1}\rangle = |1_1 0.....0\rangle$ evolves within the one excitation subspace spanned by the basis states $|\mathbf{i}\rangle = |0...01_i 0...0\rangle$. To evaluate how well an unknown initial state is transmitted, we use the transmission fidelity, averaged over all possible $|\psi_0\rangle$ from the Bloch sphere

$$F(t) \quad = \quad \frac{|f_N(t)|}{3}\cos\gamma + \frac{|f_N(t)|^2}{6} + \frac{1}{2}, \tag{3}$$

where $|f_N(t)|^2 = \left|\langle \mathbf{N}| e^{-\frac{iHt}{\hbar}} |\mathbf{1}\rangle\right|^2$ is the fidelity of transfer between states $|\mathbf{1}\rangle$ and $|\mathbf{N}\rangle$ and $\gamma = \arg|f_N(t)|$ [7]. Because the phase γ can be controlled by an external field once the state is transferred, we consider $\cos\gamma = 1$. By the symmetries of the system, this fidelity can be expressed in terms of the single-excitation energies E_k and the eigenvectors $|\Psi_k\rangle$ of H, in the following way

$$|f_N(t)|^2 = \sum_{k,s} (-1)^{k+s} P_{k,1} P_{s,1} e^{-i(E_k - E_s)t/\hbar} \tag{4}$$

where $P_{k,1} = |\langle \Psi_k | \mathbf{1}\rangle|^2$ are the eigenvector occupation probabilities on the first site of the chain.

2.2 Static disorder models

Static disorder in the couplings within the transfer channel is described by $J_i \to J_i + \Delta J_i$ ($i = 2, ..., N-2$) with ΔJ_i a random variable. We consider two possible coupling disorder models: **(a)** *relative static disorder,* where each coupling is allowed to fluctuate by a certain fraction of its ideal size, $\Delta J_i = J_i \delta_i$ [8, 10, 11, 12], and **(b)** *absolute static disorder,* where all couplings may fluctuate within a certain fixed range which we measure in terms of $J_{max} = \max J_i$: $\Delta J_i = J_{max}\delta_i$ [15, 12]. Each δ_i is an independent and uniformly distributed random variable in the interval $[-\varepsilon_J, \varepsilon_J]$. $\varepsilon_J > 0$ characterizes the strength of the disorder. The

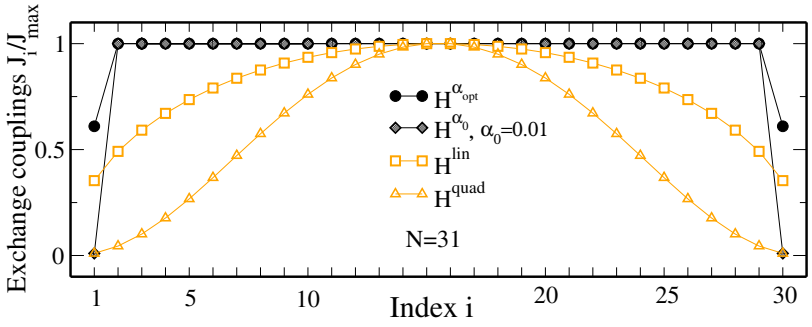

Fig. 1 (Color online) Exchange couplings $\frac{J_i}{J_{max}}$ for the boundary-controlled OST chains (black symbols) and for the fully-engineered *linear* and *quadratic* PST chains (open orange symbols). The couplings of the linear PST chain are known [25] to show a circular pattern, those for the quadratic channel are determined by solving an inverse eigenvalue problem. Chain length is $N = 31$.

two coupling disorder models are equivalent for the *boundary-controlled* spin chains since all couplings are equal there for $i = 2, ..., N-2$. However, in the fully engineered PST systems $J_{max} - J_{min}$ depends on the type of system and tends to increase with N so that absolute disorder is expected to be more damaging than relative disorder in these systems. Which kind of disorder is relevant depends on the particular experimental method used to engineer the spin chains [41].

3 Boundary controlled and fully engineered channels for robust state transfer

The boundary-controlled chains with optimizable state transfer (OST), Eqs. (1-2), can be optimized in two different ways [12]. If transmission speed is not an issue while high fidelity is desired, a weak coupling $\alpha J = \alpha_0 J \ll \frac{1}{\sqrt{N}}$ should be chosen [29, 31, 12, 32]. Perfect state transmission can then be obtained asymptotically for vanishing α but the transfer time increases with decreasing α and depends strongly on the parity of N, the spin chain length [29]. If speed is critical while fidelity need not be perfect, the boundary coupling should be optimized depending on the spin chain length, choosing $\alpha J = \alpha_{opt} J \backsimeq 1.05 N^{-\frac{1}{6}}$ [30, 31, 12]. We will denote these two cases by the symbols α_0 and α_{opt}, respectively.

The class of fully engineered spin chains with perfect state transfer (PST) is large; in fact there are countless ways to design PST-type chains [6, 40, 27]. We analyzed the performance of PST chains with power-law energy spectrum [11, 12] under the influence of static disorder. It turned out that systems with a *linear* or *quadratic* energy spectrum (see Sec. 3.1 below for details) were most robust against static disorder. The fidelity (4) of the state transfer and its robustness depend crucially on the probability $P_{k,1} = |\langle \mathbf{1} | \Psi_k \rangle|^2$ and the shape of some regions of the energy spectrum [11, 12].

In the present work we study the performance of two PST chains, denoted by ^{lin} and ^{quad}, respectively, in comparison to the OST systems $^{\alpha_{opt}}$ and $^{\alpha_0}$ introduced above. In the quadratic PST and weak-coupling OST cases the parity of N will turn out to be important [42]. This similarity, along with other similarities between OST and PST chains, can be understood from properties of the eigenstates and eigenvalues, but by no means directly from

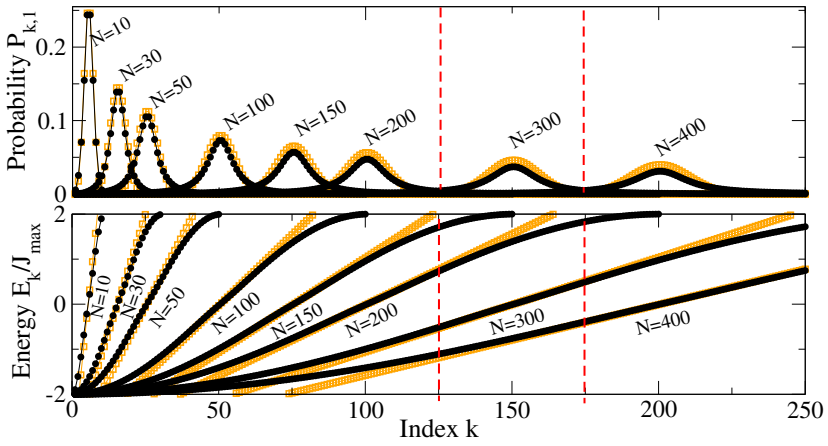

Fig. 2 (Color online) Probabilities $P_{k,1}$ to find the initial state $|\psi_0\rangle = |\mathbf{1}\rangle$ in the eigenstate $|\Psi_k\rangle$, and energies E_k of the systems $H^{\alpha_{opt}}$ (black solid dots) and H^{lin} (orange open squares) for different chain lengths N. The dashed vertical lines show, as an example for $N = 300$, the region of dominant energy eigenstates $|\Psi_k\rangle$ that contribute to the state transfer. The energy spectrum in the relevant region is linear for both systems. To stress the similarity between the energy spectra the E_k of H^{lin} have been multiplied by $\frac{\pi}{2}$.

the distribution of the couplings J_i which is shown in Figure 1.

3.1 Spectral properties

The key to high state transfer fidelity, as obvious from Eq. (4), is in the spectrum of energies E_k and the probabilities $P_{k,1}$. These quantities help to understand *(i)* similarities between ideal chains from the PST and OST classes, respectively, and *(ii)* the differences in robustness against static disorder. Note that *(i)* is significant in terms of experimental feasibility, since OST-chains are potentially easier to manufacture than PST-chains.

The single-excitation energy eigenvalues of the systems considered are given as follows:

(a) for OST-chains, $E_k = 2J\cos\gamma_k$, where k is given by the N solutions of $\pm\cot\gamma_k\,\cot^{\pm1}(\frac{N-1}{2}\gamma_k) = \frac{\alpha^2J^2}{2-\alpha^2J^2}$ [29]; and

(b) for PST-chains, $E_{\tilde{k}} = \frac{\pi\hbar}{\tau_{pst}}\mathrm{sgn}(\tilde{k})|\tilde{k}|^m$, where $\tilde{k} = -\frac{N-1}{2}, ..., \frac{N-1}{2}$ and the exponent $m = 1$ for the *linear* case and $m = 2$ for the *quadratic* one, for odd N. If N is even, $\tilde{k} = -\frac{N}{2}, ..., \frac{N}{2}$, excluding zero, and in the linear (quadratic) case, $|\tilde{k}|$ ($|\tilde{k}|^2$) has to be replaced by $|\tilde{k}| - \frac{1}{2}$ $\left(|\tilde{k}^2 - \frac{1}{2}|\right)$ in $E_{\tilde{k}}$. Here, τ_{pst} is the time after which the first perfect state transfer occurs.

A common property of all these systems that makes them robust is that the eigenstates involved in the state transmission belong to the center of the energy band [11, 12]. The α_{opt}-OST chain has a linear spectrum in this energy region as shown in Fig. 2 for several chain lengths N. In contrast, the α_0-OST chain has a rather flat spectrum there, similar to the *quadratic*-PST channel as shown in Fig. 3.

At the same time, the probability of the k-th energy eigenstate to participate in the state transfer is given by $P_{k,1}$, Eq. (4). For

(a) OST-chains, $P_{k,1}^{\alpha_{opt}}$ is a Lorentzian distribution [34] while $P_{k,1}^{\alpha_0}$ is essentially non-zero

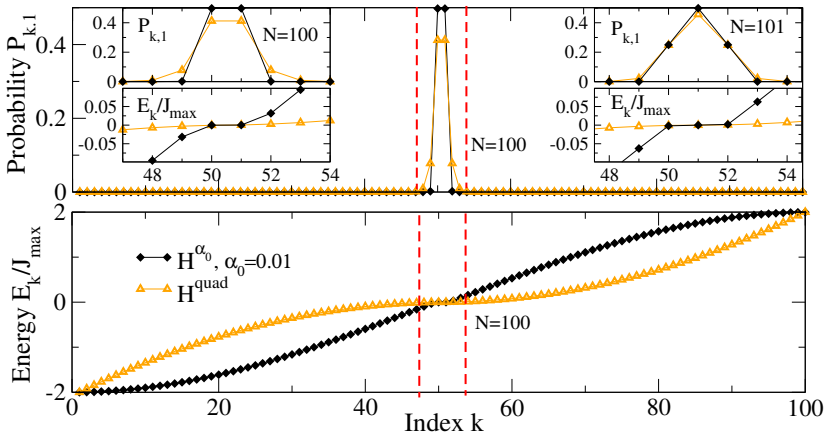

Fig. 3 (Color online) Probabilities $P_{k,1}$ to find the initial state $|\psi_0\rangle = |\mathbf{1}\rangle$ in the eigenstate $|\Psi_k\rangle$ and energies E_k of the system H^{α_0} ($\alpha = 0.01$; black solid diamonds) and H^{quad} (orange open triangles) for even $N = 100$. The dashed vertical lines show the small region of dominant energy eigenstates $|\Psi_k\rangle$ that contribute to the state transfer. This region is shown magnified in the left inset. The right inset shows the same for odd $N = 101$.

only for two (three) values of k when N is even (odd) [29] (Fig. 3); whereas for

(b) PST-chains, $P^{lin}_{k,1}$ follows a Gaussian distribution (see Appendix 1) while $P^{quad}_{k,1}$ is significantly different from zero only for two (three) values of k when N is even (odd) (Fig. 3). The significant contributions of $P_{k,1}$ for all the above channels are thus all concentrated near the center of the energy band. The varying degree of that concentration naturally separates the four systems into two pairs: The α_{opt} and linear systems show a broad $P_{k,1}$ distribution (Fig. 2), whereas in the α_0 and quadratic systems, $P_{k,1}$ is very narrow. Given the similarities in the relevant parts (as determined by $P_{k,1}$ being of appreciable size) of the energy spectra E_k, it is clear that the members of each pair can be expected to show very similar behavior.

Figure 2 shows clearly the mechanism behind the high state transfer fidelities shown by the two systems represented there. While it takes a relatively large number of energy eigenstates $|\Psi_k\rangle$ to resolve the localized initial state $|\psi_0\rangle$, the eigenvalues E_k of those states are equidistant due to the linear spectrum. That makes the time evolution of the initial state periodic with a period equal to twice the time needed for the state transfer from site 1 to site N. Spatial symmetry then is the second ingredient needed to provide for perfect or near-perfect state transfer. The probability distributions $P_{k,1}$ in Fig. 2 are known. $P^{\alpha_{opt}}_{k,1}$ was shown to be Lorentzian [34]:

$$P^{\alpha_{opt}}_{k,1} \simeq \frac{1}{\pi}\frac{\Gamma}{(k-k_0)^2+\Gamma^2}, \tag{5}$$

where $k_0 = \frac{N+1}{2}$ and $\Gamma \simeq (\frac{10}{N})^{-0.63}$ (best fit for $N = 400$). $P^{linear}_{k,1}$ is asymptotically Gaussian (see Appendix 1)

$$P^{linear}_{k,1} \simeq Ae^{-\frac{(k-k_0)^2}{2\sigma^2}}, \tag{6}$$

with $A = \frac{0.8}{\sqrt{N}}$ and $\sigma = \frac{2}{\sqrt{N}}$ (for $N = 400$).

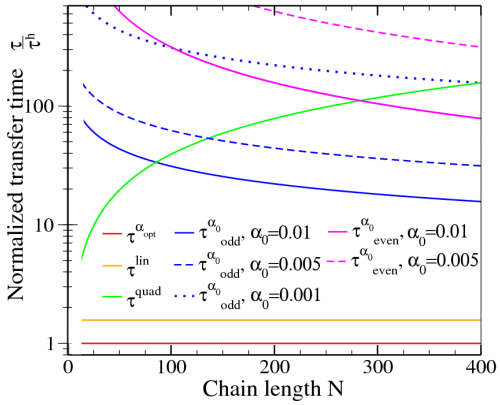

Fig. 4. (Color online) Transfer times τ where the maximum transfer fidelity is achieved as a function of N and α_0. τ^h is the transfer time for a homogeneous chain, *ie.* $J_i = J\ \forall J_i$. Values $\frac{\tau}{\tau^h}(N, \alpha_0)$ are given for $\alpha_0 = 0.001, 0.005, 0.01$.

The α_0-OST and *quadratic*-PST systems from Fig. 3 are quite different. There the state transfer is performed by a very small (and N-independent) number of eigenstates. For even N, in the limit $\alpha_0 \to 0^+$ the dominant eigenvectors belong to the two energies $E_{k_\pm} = \pm|E|_{min}$ closest to zero, that is, $|\Psi_{k_\pm}\rangle$ with $k_- = \frac{N}{2}$, $k_+ = \frac{N}{2} + 1$. The probabilities for these states are $P^{\alpha_0}_{k_\pm,1} \simeq \frac{1}{2}$, and, by normalization $P^{\alpha_0}_{k,1} \simeq 0$ for $k \neq k_\pm$. For odd N, in contrast, three eigenvectors, $|\Psi_{k_\pm}\rangle$ and $|\Psi_{k_0}\rangle$ (with $E^{\alpha_0}_{k_0} = 0$) are dominant, with $P^{\alpha_0}_{k_\pm,1} \simeq \frac{1}{4}$ and $P^{\alpha_0}_{k_0,1} \simeq \frac{1}{2}$. The nonzero energy eigenvalues for small α_0 are very different: $E^{\alpha_0}_{k_\pm,even} \sim \pm\alpha_0^2$ and $E^{\alpha_0}_{k_\pm,odd} \sim \pm\frac{2\alpha_0}{\sqrt{N}}$ [29]. For *quadratic*-PST systems we numerically observe a similar behavior with the addition of a small contribution from two more eigenstates, those belonging to the pair of energies next closest to zero.

We have analyzed the changes in both the energy spectrum E_k and the structure of the eigenstates, as displayed by the probabilities $P_{k,1}$, under the influence of disorder [11, 42]. As a general rule it turns out that energies near the center of the energy band are least affected by disorder in the class of spin chains discussed here. Since the band-center states are most important for state transfer, this sounds like a piece of good news. Of all systems, H^{quad} shows the smallest "spectral sensitivity", as measured by the standard deviation of E_k for given disorder strength ε_J. However, since both the energy eigenvalues and the occupation probabilities $P_{k,1}$ influence the fidelity, this does not mean that H^{quad} is the most robust state transfer system under all circumstances. Quite to the contrary, H^{quad} tends to be rather robust for odd N and quite delicate for even N; see Section 4.2 for details.

Below we shall discuss the performance of all channels as measured by the transfer time and the transfer fidelity (3) and we shall observe marked similarities between the members of each of the two pairs of state transfer channels. These similarities can be explained by the features of the eigenvalues E_k and probabilities $P_{k,1}$ just discussed.

Homog	α-OST channel			PST channel	
$\tau^h \simeq \frac{N}{2J_{max}}$	$\tau^{\alpha_{opt}} \gtrsim \frac{N}{2J_{max}}$	$\tau^{\alpha_0}_{odd} \simeq \frac{\pi\sqrt{N-2}}{2\alpha J_{max}}$	$\tau^{\alpha_0}_{even} \simeq \frac{\pi}{2\alpha^2 J_{max}}$	$\tau^{lin} \simeq \frac{\pi N}{4J_{max}}$	$\tau^{quad}_{odd,even} \simeq \frac{\pi N^2}{8J_{max}}$
$\simeq \tau^h$	$\gtrsim \tau^h$	$\simeq \frac{\pi\sqrt{N-2}}{\alpha N}\tau^h$	$\simeq \frac{\pi}{\alpha^2 N}\tau^h$	$\simeq \frac{\pi}{2}\tau^h$	$\simeq \frac{\pi N}{8}\tau^h$

Table 1. Transfer times τ where the maximum of the fidelity of transmission is obtained for different spin chains. The last row compares these times with the transfer time τ^h of a homogeneous chain, *ie.* $J_i = J\ \forall J_i$. The transfer time τ^{lin} was obtained in Ref. [25], τ^{α_0} in Ref. [29], $\tau^{\alpha_{opt}}$ in Ref. [31] and we obtained $\tau^{quad}_{odd,even}$ from our numerical results.

4 Performance comparison: Transfer time and fidelity

4.1 The transfer time

There is no unique way to define the transfer time for arbitrary state transfer channels, since the fidelity as a function of time may show a complicated pattern of maxima [11]. As a working definition we may say that the transfer time is defined by the first maximum of useful size in the fidelity. In the examples discussed here the fidelity does not show erratic dynamics and the meaning of the transfer time will be unambiguous. The transfer time τ depends strongly on the type of spin chain [29, 43, 22, 11, 31]. PST channels have commensurate energies E_k; that means, all transition frequencies share a common divisor τ_{PST} to make $f_N = 1$ in Eq. (4) [25, 6]. In particular, the times τ^{lin} and τ^{quad} for *linear* and *quadratic* PST channels are half of the mesoscopic echo time [11], which is the characteristic (round-trip) time of the information propagation within the chain. For other systems the transfer time is generally longer [11]. For some PST chains the exact transfer time can be obtained analytically [6, 5, 25, 28, 11]. For other types of chains, such as the boundary-controlled ones considered in this work, the transfer time must be obtained by *ad hoc* means [29, 34, 31].

The transfer times for the chains considered here are listed in Table 1. The shortest transfer time is achieved by the boundary-controlled chain working in the *optimal* regime [12]. This transfer time is very close to the bound given by the quantum speed limit $\tau^h = \frac{N}{2J_{max}}$ given by the maximum group velocity of excitations in the homogeneous chain [44, 43, 45, 22]. The transfer times for different channels are given in units of τ^h in the last row of Table 1. The shortest time $\tau^{\alpha_{opt}}$ is followed by τ^{lin}, and then by the remaining transfer times, τ^{α_0} and τ^{quad} which depend on N and α_0 as shown in Fig. 4. If $\alpha_0 \ll \frac{1}{\sqrt{N}}$, we always have $\tau^{\alpha_0}_{odd} < \tau^{\alpha_0}_{even}$ and for $\alpha \lesssim \frac{8\sqrt{N-2}}{N^{3/2}}$, $\tau^{quad} < \tau^{\alpha_0}_{odd}$.

A comparison of the transfer fidelity as a function of time in the absence of disorder is displayed in Fig. 5. We can observe there the basic characteristics of each channel. In particular, in Fig. 5a we observe the faster transfer of the α_{opt}-OST channel as compared to the *linear* one, while its fidelity maximum is lower than that of the *linear* PST-channel. For the α_0-OST and the *quadratic* PST channels, the transfer is slower than in the previous cases and it depends on the parity of the chain length. This is because for odd N the transmission of the state from the boundary spins is mainly performed through an eigenstate of the bulk spins ($i=2,..,N-1$) that is in the center of the band ($E_k = 0$) and consequently on resonance with the boundary spins [29, 32]. However, for even N, the transfer proceeds through two eigenstates of the bulk spins with finite energy and consequently off-resonance with the boundary spins [29, 32]. The fast oscillation observed in the inset of Fig. 5c for F^{α_0} with even N is an evidence of the off-resonance transmission. A simple calculation

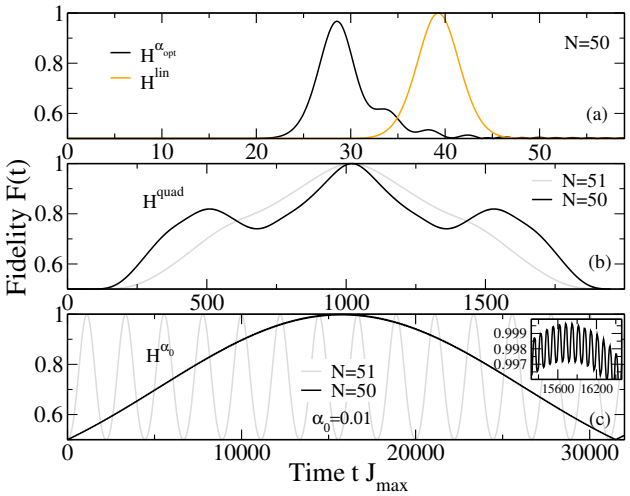

Fig. 5. (Color online) Transmission fidelity $F(t)$ as a function of time t. **(a)** $F^{\alpha_{opt}}(t)$ (black line) and $F^{lin}(t)$ (orange line) for an even chain length $N = 50$. The behavior of the fidelity is not affected by the parity of N. However, for **(b)** $F^{quad}(t)$ and **(c)** $F^{\alpha_0}(t)$, the parity of N matters. Panels (b,c) show the fidelity for $N = 50$ (black line) and $N = 51$ (gray line). The inset in (c) shows the oscillation observed for even N that is an evidence of the off-resonance transmission which is much slower than the on-resonance transmission for odd N.

considering the dynamics in the space spanned by the dominating eigenstates reveals the frequency of the oscillation that varies with N as $\omega_{\alpha_0} \sim \frac{\pi J_{max}}{N}\sqrt{\alpha_0^2 N + 1}$ and the amplitude as $A_{\alpha_0} \sim \frac{1}{4}\alpha_0^2 N(N\alpha_0^2 + 1)^{-1}$. The main slower oscillation that produces the state transfer comes from only two eigenvectors of the total system ($i = 1, .., N$) strongly localized in the channel's ends [29]. For odd N the transmission is smooth because it proceeds through the eigenstate with zero energy. A similar behaviour with respect to the parity of N is also observed in the *quadratic*-PST channel.

A second important time scale apart from the transfer time is what one may call the window-time, that is, the width of the fidelity maximum which defines the transfer time. That time scale defines the precision in time that is needed to read out the state transferred with high fidelity. While the *quadratic* and α_0 channels are slower in transfer than their *linear* and α_{opt} counterparts, they have the widest window of time. The achievable transfer fidelity at time τ will be discussed below, when we deal with state transfer in the presence of imperfections.

4.2 The transfer fidelity under disorder

As we mentioned in the introduction, for a set of manufactured quantum spin chains, the best-case, worst-case, or average fidelities may be relevant, depending on the situation at hand. When dealing with disordered chains the particular realization of the disorder present in the chain is unknown, unless a complete tomography of the Hamiltonian can be carried out. Since the situation we imagine is a future "integrated quantum circuit" with a large number of quantum gates and a correspondingly large number of spin chains connecting gates and registers, the complete tomography of the multi-chain Hamiltonian is extremely cumbersome. In that case the average fidelity will be most relevant in order to compare different protocols

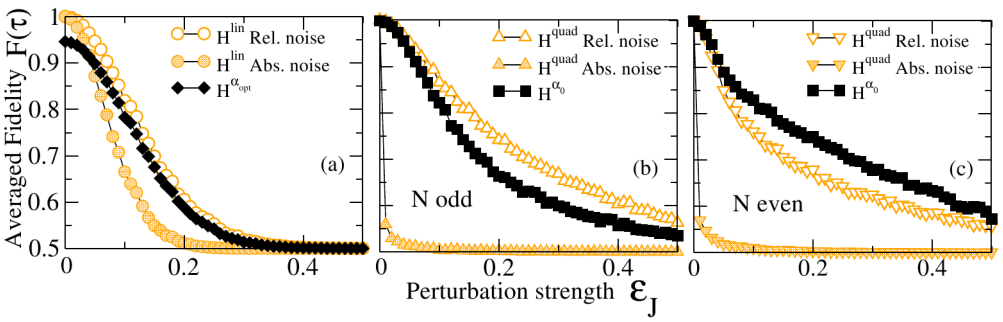

Fig. 6. (Color online) Averaged fidelity at time τ as a function of the perturbation strength ε_J for OST and PST channels for a given chain length N. Relative and absolute static disorder are considered. (a) $\overline{F}^{lin}$ with relative disorder (open circles) and absolute disorder (filled orange circles) and $\overline{F}^{\alpha_{opt}}$ (black diamonds) for both kinds of disorder when $N = 200$. (b) $\overline{F}^{quad}$ with relative disorder (open triangles) and absolute disorder (filled orange triangles) and $\overline{F}^{\alpha_0}$ (black squares, $\alpha_0 = 0.01$) for both kinds of disorder when $N = 200$. (c) Same as panel (b) for $N = 201$. The fidelity was averaged over $N_{av} = 10^3$ realizations of the disorder in each case.

and obtain general results. Therefore, we consider the average of the fidelity (3), evaluated at time τ, over N_{av} realizations of the disorder,

$$\overline{F}(\tau) = \langle F(\tau) \rangle_{N_{av}} . \tag{7}$$

All following numerical simulations employ $N_{av} = 10^3$ realizations for the disorder.

Figure 6 shows the typical behavior of the averaged fidelity, $\overline{F}(\tau)$, for the different kinds of channels and disorders here considered, as a function of the disorder strength. For a fixed length N, the averaged fidelity $\overline{F}(\tau)$ is a decreasing function of the disorder strength. The panels are grouped according to the similarities observed in the spectral properties of the different systems as discussed above. Obviously, these similarities are reflected in the performance of the transfer fidelity when relative noise is considered. For absolute noise, the disorder is more detrimental for PST systems since $\frac{J_{max}}{J_{min}}$ can be a large number. A detailed analysis of Fig. 6 and the comparison of robustness in these systems follows below.

Figure 7 shows the averaged fidelity as a function of the disorder strength ε_J and of the chain length N for all the channels considered.

The contour lines are defined by $\overline{F}(\tau) = const.$ values. With the exception of the region where $\overline{F}^{\alpha_{opt}} > 0.9$, we observe a very general behavior of the averaged fidelity for the region of interest: the curves $\overline{F} = const.$ are straight lines in the logarithmic (ε_J, N) plane, *i.e.* the contour lines of the surface $\overline{F}(\tau)\,[\varepsilon_J, N]$ are curves given by $N\varepsilon_j^{\beta} = const.$. We did not attempt to derive general scaling laws for the systems studied here. Instead we provide a simple phenomenological description of the numerical results in a certain range of perturbation strengths and chain lengths. That range is determined by fidelity values which might be relevant for state transfer, thus allowing to quantitatively compare the performances of different channels. Thus, by fitting the averaged fidelities in this region of interest, we found for all the channels involved in Fig. 6, the scaling function

$$\overline{F}(N, \varepsilon_J) = \overline{F}(N\varepsilon_J^{\beta}) = \frac{1}{2}\left[1 + e^{-cN\varepsilon_J^{\beta}}\right], \tag{8}$$

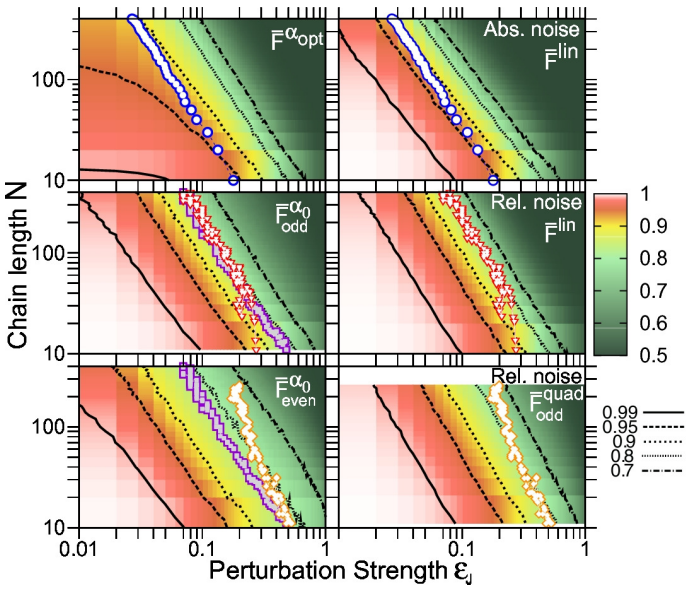

Fig. 7. (Color online) Averaged fidelity $\overline{F}^{\alpha_{opt}}$,$\overline{F}^{\alpha_0}_{even}$,$\overline{F}^{\alpha_0}_{odd}$, and $\overline{F}^{lin}$ when both kinds of disorder are considered and $\overline{F}^{quad}_{odd}$ when only *relative disorder* is considered. The average is calculated over $N_{av}=10^3$ realizations in each case. The black contour lines belong to $F=0.99$, 0.95, 0.9, 0.8, 0.7, respectively. The colored symbols show the crossovers between the different systems as explained in the text.

where c is a positive constant. Table 2 gives the values of the exponent β and the prefactor c for the different channels. We note that for strong perturbations the spoiled transfer can be associated to dynamical localization effects (e.g. Anderson localization) [46, 47, 48]. These localization effects are related to zero-velocity Lieb Robinson bounds, which in XX chain systems lead to the bound $|f_N(t)| \leq Ce^{-\eta(\varepsilon_J)d(N)}$, where $\eta(\varepsilon_J)$ is associated with the disorder strength and $d(N)$ with the site-distance between boundary spins [46]. That yields a functional form (similar to (8)) for a bound of the averaged fidelity $\overline{F}(t) \leq \frac{1}{2}+\frac{Ce^{-\eta(\varepsilon_J)d(N)}}{3}+\frac{C^2e^{-2\eta(\varepsilon_J)d(N)}}{6}$.

The scaling function (8) for $\overline{F}^{lin}$ with values $\beta = 2$ and $c = \frac{1}{5}$ has been reported previously in Ref. [8], derived from a perturbative analysis. The deviation of the numerical values $F^{\alpha_{opt}} > 0.9$ from the simple scaling function (8) can be understood remembering that the *optimal* channels do not ever achieve $\overline{F} = 1$. Note that $\overline{F}^{\alpha_0}_{even}$ starts to deviate faster than $\overline{F}^{\alpha_0}_{odd}$ from the straight lines when the disorder strength is reduced for large N. That can be attributed to the fast oscillations described in Sec. 4.1 due to the off-resonance transmission. The oscillations induce fluctuations over realizations that are around twice the oscillation's amplitude, $2A_{\alpha_0}$, which increases with N.

The data analyzed so far in this section suggest that there is no single simple answer to the question which spin chain is most adequate to achieve quantum state transfer for a given disorder model. In the following we try to answer this question in some more detail.

Optimal coupling regime α_{opt}-OST vs. linear-PST channels

Considering *relative* disorder, the main difference between the systems occurs in the region $\varepsilon_J \sim 0$, as can be well observed in Fig. 6a, because the case α_{opt}-OST does not produce

	$\alpha - OST$channels			PSTchannels			
	$F^{\alpha_{opt}}$	$F^{\alpha_0}_{odd}$	$F^{\alpha_0}_{even}$	F^{lin}		F^{quad}_{odd}	F^{quad}_{even}
	Abs. and Rel. noise			Rel. noise	Abs. noise	Rel. noise	
c	0.21	0.17	0.29	0.21	0.20	0.26	0.51
β	1.907	1.887	1.81	2.00	1.634	2.14	1.89

Table 2. Values of the constant c and the exponent β for the scaling law $\overline{F}(N\varepsilon_J^\beta) = \frac{1}{2}\left[1+e^{-cN\varepsilon_J^\beta}\right]$. These values come from the fit parameters of the contour lines displayed in Fig. 7, which then are averaged to obtain a representative value for each of the different systems. Only the contour lines that can be well fitted by a straight line are considered. Thus, the scaling law for $F^{\alpha_{opt}}$ is defined by considering the contour lines with $F^{\alpha_{opt}} \leq 0.8$.

PST in the limit of zero disorder, i.e., $\overline{F}^{lin} \gtrsim \overline{F}^{\alpha_{opt}}$. For stronger disorder, both fidelities are similar and thus engineering might not be necessary in that regime. The fidelity's functional dependence on ε_J and N for the *linear*-PST channel is $\overline{F}^{lin}(N\varepsilon_J^2) \approx \frac{1}{2}\left[1+e^{-\frac{1}{5}N\varepsilon_J^2}\right]$ [8] as shown in Fig. 7d. In contrast, the α_{opt}-OST channel shows two regimes depending on ε_J. Within the range of ε_J and N covered in Fig. 7, the boundary between the two regimes is given by $\varepsilon_J^0 \approx (\frac{1.65}{N})^{0.66}$ and a fidelity value of $\overline{F}^{\alpha_{opt}}_{\varepsilon_J^0} = 0.91$. For $\varepsilon_J > \varepsilon_J^0$ the average fidelity of the α_{opt}-OST system scales with $N\varepsilon_J^\beta$ but β varies from 1.61 to 1.91. For smaller disorder, $\varepsilon_J < \varepsilon_J^0$, the behavior is different as it should, since the α_{opt} system never reaches perfect fidelity at zero disorder. The fidelity difference between the two systems at ε_J^0 is quite small: $\Delta\overline{F} = \overline{F}^{lin}_{\varepsilon_J^0} - \overline{F}^{\alpha_{opt}}_{\varepsilon_J^0} \approx \frac{1}{100}(3\log N - 2)$; in numbers that means $0.004 \leq \Delta\overline{F} \leq 0.058$.

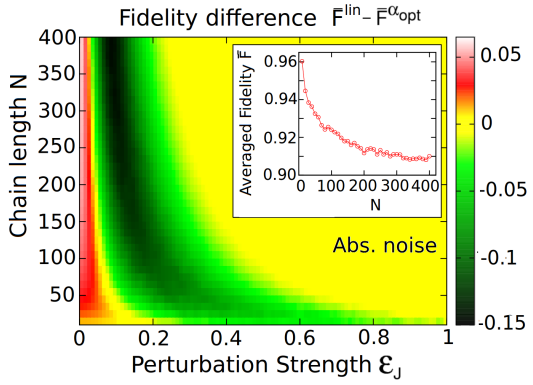

Fig. 8. (Color online) Averaged fidelity difference $\Delta\overline{F} = \overline{F}^{lin} - \overline{F}^{\alpha_{opt}}$ at time τ as a function of the perturbation strength ε_J and the chain length N, averaged over $N_{av} = 10^3$ realizations and with *absolute disorder*. The points where $\Delta\overline{F} = 0$ in the (N, ε_J) plane are shown as circles in Figs. 7a and 7b. The inset shows the value of the fidelity at the crossing point $\Delta\overline{F} = 0$, as a function of N.

Considering now *absolute* static disorder, in Fig. 6a we can see that the *linear*-PST system performs better than α_{opt}-OST only for weak perturbations ε_J. For stronger perturbations the α_{opt}-OST system overcomes the *linear*-PST performance. Studying this behavior as a function of N as shown in Fig. 7a and b, we can see that the crossing point when $\overline{F}^{lin} - \overline{F}^{\alpha_{opt}} = 0$ is determined by $N\varepsilon_J^{1.91} \approx 0.43$ shown as empty blue circles in Fig. 7. For the *linear*-PST channel with absolute disorder the contour lines of the fidelity are given by $N\varepsilon^{1.63}$ instead of

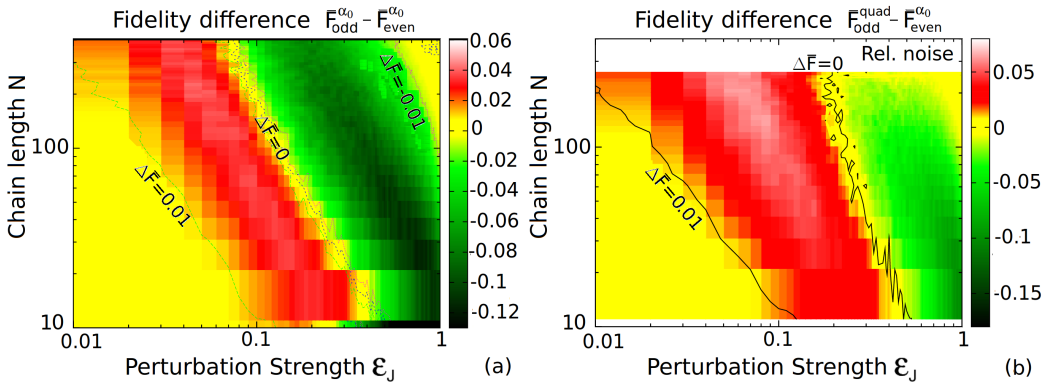

Fig. 9. (Color online) Averaged fidelity differences $\Delta\overline{F}$ at time τ as a function of the perturbation strength ε_J and the chain length N, averaged over $N_{av} = 10^3$ realizations. **(a)** $\overline{F}^{\alpha_0}_{odd} - \overline{F}^{\alpha_0}_{even}$. The violet squares in Fig. 7c and 7d show $\Delta\overline{F}(N, \varepsilon_J) = 0$. **(b)** $\overline{F}^{quad}_{odd} - \overline{F}^{\alpha_0}_{even}$ with *relative disorder*. The orange diamonds in Fig. 7e and 7f display $\Delta\overline{F}(N, \varepsilon_J) = 0$.

$N\varepsilon^2$ in the case of relative disorder, while for the minimally engineered α_{opt}-OST channel the scaling behavior remains the same, as argued earlier.

Figure 8 shows the difference $\overline{F}^{lin} - \overline{F}^{\alpha_{opt}}$ and the value of the fidelity at the crossing point is shown in the inset. It varies from 0.96 for $N = 10$ to 0.91, for $N = 400$. This demonstrates that when N increases, the region where the *linear*-PST channel performs better is reduced and if the perturbation is not small enough, the minimally engineered α_{opt}-OST channel performs better. As expected, the *linear*-PST channel when suffering *absolute disorder* is strongly affected as compared to *relative disorder* where the commensurability of the energy levels is less strongly disturbed by the disorder. With all of this analysis, we can identify regions in terms of physical quantities and different disorder models where the α_{opt}-OST performs better than the *linear*-PST transfer or vice versa. While the α_{opt}-OST system is always faster in terms of transfer time, the quality of the transfer is sometimes lower. However, this difference of fidelity is more appreciable for small perturbations and short chains. In the other cases, the α_{opt}-OST system can be more robust.

Weak coupling regime α_0-OST vs. quadratic-PST channels

Considering *relative disorder*, the fidelity of the boundary-controlled α_0-OST system $\overline{F}^{\alpha_0}$ is similar or higher (lower) than that of the *quadratic*-PST channel $\overline{F}^{quad}$ when N is even (odd), *ie.* $\overline{F}^{\alpha_0}_{even} \gtrsim \overline{F}^{quad}_{even}$ and $\overline{F}^{\alpha_0}_{odd} \lesssim \overline{F}^{quad}_{odd}$ (see Figs. 6b and 6c). The better performances $\overline{F}^{\alpha_0}_{even}$ and $\overline{F}^{quad}_{odd}$ are shown in Fig. 7e and 7f respectively. The orange diamond symbols there indicate where these fidelities are equal, *ie.* $\overline{F}^{\alpha_0}_{even} = \overline{F}^{quad}_{odd}$, a fit gives $N\varepsilon_J^{3.5} \approx 0.62$ and the fidelity value is around $F \approx 0.8$, decreasing for larger N. To the left of the symbols $\overline{F}^{quad}_{odd} > \overline{F}^{\alpha_0}_{even}$, but for small perturbation strength the differences between the two systems are quite small as visible in Fig. 9b.

The fidelity contour lines $\overline{F}^{\alpha_0}_{even} = \text{const}$ do not follow the scaling $N\varepsilon_J^{\beta} \sim \text{const}$ for values below 0.8. In this region, the effect of the perturbation depends on α_0, but only for even N. That is shown in Fig. 10 which also demonstrates marked differences between even and odd N in the dependence of $\overline{F}^{\alpha_0}(\tau)$ on ε_J. Note, however, that the differences are most conspicuous

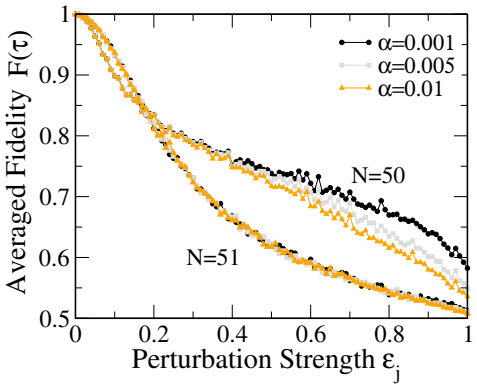

Fig. 10. (Color online) Averaged transfer fidelity F^{α_0} as a function of the perturbation strength ε_J and the coupling strength α_0 for relative disorder. The dependence on α_0 is only appreciable for even number of spins N in the chain.

in the region where the fidelity is much too small anyway for reliable quantum information processing.

Considering *absolute disorder*, the minimally engineered H^{α_0} systems are always the most robust ones for transferring information. The fidelity of H^{quad} in that case decays very rapidly as a function of N and ε_J (not shown). This is connected to the fact that the maximum and minimum couplings, J^{quad}_{max} and J^{quad}_{min}, in the chain may differ by orders of magnitude, with the smallest couplings always close to the ends of the chain $J^{quad}_{min} = J^{quad}_1 = J^{quad}_N$. We found a relation $\frac{J^{quad}_{max}}{J^{quad}_{min}} \sim 0.06N^2$ for even N and $\sim 0.1N^2$ for odd N. Consequently, a fluctuation of a given absolute size may completely spoil the state transfer when it affects one of the small couplings close to the boundary as observed in Figs. 6b and 6c for $N = 200$.

Returning to the α_0-OST channels, in Figs. 7c and 7e we can compare the fidelities $\overline{F}^{\alpha_0}_{odd}$ and $\overline{F}^{\alpha_0}_{even}$. The violet squares show when $\overline{F}^{\alpha_0}_{odd} = \overline{F}^{\alpha_0}_{even}$, where $\overline{F}^{\alpha_0}_{odd} > \overline{F}^{\alpha_0}_{even}$ to the left of the symbols. This crossing line approximately follows $N\varepsilon_J^{1.98} \approx 0.50$ and corresponds to a constant fidelity value $F^{\alpha_0} \gtrapprox 0.8$. The differences between these fidelities are displayed in Fig. 9a.

Minimally engineered vs. fully engineered channels

Comparing all of the systems for *relative disorder*, for small perturbation, most of the systems achieve a high fidelity of state transfer. In general we observe in Fig. 11 that for fidelities $\gtrsim 0.8$, where the functional dependence of the infidelity $1-\overline{F}$ as a function of the perturbation strength is quadratic for all systems with $\overline{F} \to 1$ for $\varepsilon_J \to 0$, the most robust system is H^{quad}_{odd} and the least robust one H^{quad}_{even}. This means that the contour lines in the (N, ε_J) plane are bounded by the ones belonging to H^{quad}_{odd} from above and by those for H^{quad}_{even} from below. For $F > 0.8$ the most robust system is H^{quad}_{odd}, but the H^{linear} system follows with very similar performance, although the $H^{\alpha_0}_{odd}$ system is also comparable since their fidelities, $\overline{F}^{lin}$ and $\overline{F}^{\alpha_0}_{odd}$, differ only by 4% or less as ε_J and N increase. In Fig. 7c and 7d, the red down-triangle symbols show where $\overline{F}^{lin} = \overline{F}^{\alpha_0}_{odd} \approx 0.8$. When $N\varepsilon_J^{1.93} \gtrsim 2.58$, $\overline{F}^{\alpha_0}_{odd} > \overline{F}^{lin}$. The different behaviors and regimes just mentioned can be seen from Fig. 11 where contour lines corresponding to several values of the averaged fidelities for all the systems are shown.

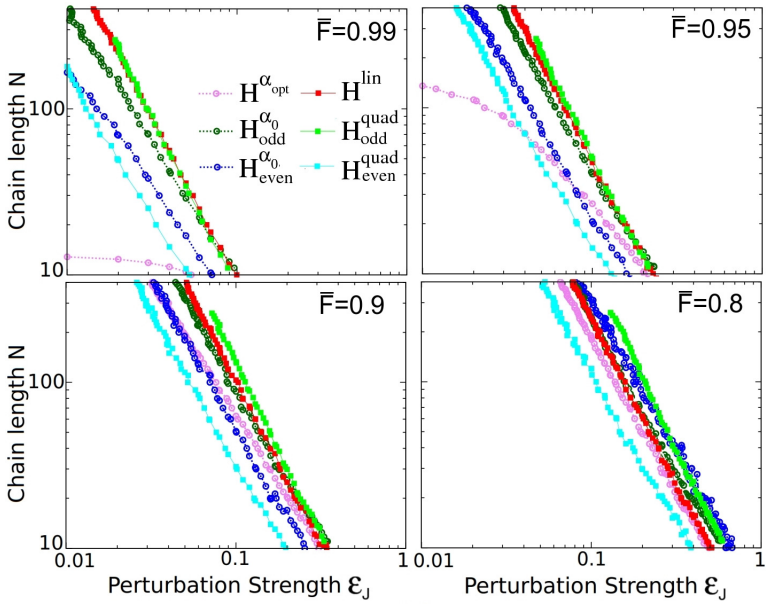

Fig. 11. (Color online) Contour lines of the averaged transfer fidelity for fully-engineered perfect state transfer systems (closed symbols) and boundary-controlled α-optimized state transfer systems (open symbols) for relative noise. They are shown as a function of the perturbation strength ε_J and the chain length N for the averaged fidelities $\overline{F} = 0.99, 0.95, 0.9, 0.8$.

For *absolute disorder*, the minimally engineered quantum channels are clearly most robust against perturbations. In this case, H^{α_0} is most robust. See the previous section for the comparison of the fidelities $\overline{F}^{\alpha_0}_{odd}$ and $\overline{F}^{\alpha_0}_{even}$. Only for small perturbation the best $\overline{F}^{lin}$ performance is similar to $\overline{F}^{\alpha_0}$ as can be seen in Figs. 12a and 12b.

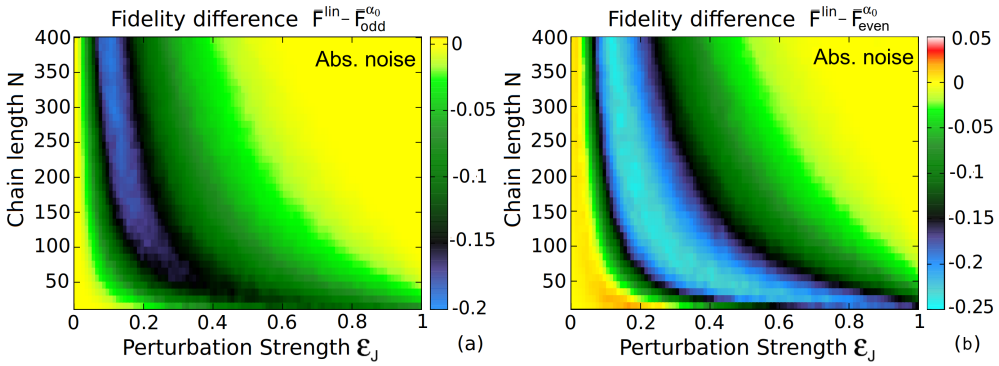

Fig. 12. (Color online) Averaged fidelity differences $\Delta\overline{F}$ at time τ as a function of the perturbation strength ε_J and the chain length N, averaged over $N_{av} = 10^3$ realizations. *Absolute disorder* is considered for **(a)** $\overline{F}^{lin} - \overline{F}^{\alpha_0}_{odd}$ and **(b)** $\overline{F}^{lin} - \overline{F}^{\alpha_0}_{even}$.

In terms of the transfer time, the fastest transfer is achieved almost at the quantum speed limit [22] by the α_{opt}-OST system, then follows the *linear*-PST system, and the transfer times of the remaining systems depend on the values of N and α, where always $\tau^{\alpha_0}_{odd} \leqslant \tau^{\alpha_0}_{even}$ and

for $\alpha \lesssim \frac{8\sqrt{N-2}}{N^{3/2}}$, $\tau^{quad} < \tau^{\alpha_0}_{odd}$.

5 Conclusions

We studied the robustness of nearest-neighbor coupled spin chains for state transfer against different kinds of static coupling-constant disorder. We identified perfect state transfer (PST) channels that are robust against static disorder in the coupling strength. We found and showed similarities in the spectral properties that are responsible for the dynamics of the transfer for some minimally engineered channels on the one hand, those that we call boundary-controlled channels, and fully engineered PST channels on the other hand. We showed that these minimally engineered systems perform similarly to fully engineered systems. We conclude that in many situations, the minimally engineered channels are similar to or even more efficient and robust in presence of perturbations than the fully engineered channels. This points out possibilities to circumvent the obvious difficulties inherent in implementing experimentally a fully engineered system with nearest-neighbor couplings which vary over orders of magnitude within the system. Moreover, one of the minimally engineered systems (the α_{opt}-OST channel) achieves the fastest state transfer.

Additionally, we documented a common decay law for the transfer fidelity, $\overline{F}(N\varepsilon_J^\beta) = \frac{1}{2}\left[1 + e^{-cN\varepsilon_J^\beta}\right]$, as a function of the perturbation strength ε_J and the channel length N, where the exponent β turns out to be close to 2 for all systems in the parameter range studied for the different systems. This law quantifies the sensitivity and robustness against perturbations. The parameters of these scaling laws which we provide for the different proposed quantum channels can serve to judge which configuration would be optimal for realizing state transfer in a given situation. While the exponent $\beta = 2$ can be derived from a perturbative treatment [8], there is no straightforward explanation for the deviations from that integer exponent value. On one hand, for the (minimally engineered) OST cases, the fidelity scaling law may deviate from that simple form due to the fidelity not being perfect for vanishing disorder strength. On the other hand, for strong disorder, dynamical localization effects may influence the scaling laws [46].

Acknowledgements

A. Z. and O. O. acknowledge support from SECYT-UNC and CONICET. A.Z. thanks for support by DAAD. GAA acknowledges the support of the European Commission under the Marie Curie Intra-European Fellowship for career Development.

References

1. M. A. Nielsen, I. L. Chuang, *Quantum computation and quantum information*, Cambridge Univ. Press, Cambridge, **2001**.
2. D. P. DiVincenzo, *Fortsch. Physik* **2000**, *48*, 771.
3. S. Bose, *Contemp. Phys.* **2007**, *48*, 13–30.
4. G. Nikolopoulos, I. Jex (Eds.), *Quantum State Transfer and Quantum Network Engineering*, Springer Series in Quantum Science and Technology, Springer, Berlin, **2014**.
5. C. Albanese, M. Christandl, N. Datta, A. Ekert, *Phys. Rev. Lett.* **2004**, *93*, 230502.
6. P. Karbach, J. Stolze, *Phys. Rev. A* **2005**, *72*, 030301.
7. S. Bose, *Phys. Rev. Lett.* **2003**, *91*, 207901.
8. G. De Chiara, D. Rossini, S. Montangero, R. Fazio, *Phys. Rev. A* **2005**, *72*, 012323.

9. J. Allcock, N. Linden, *Phys. Rev. Lett.* **2009**, *102*, 110501.
10. D. Petrosyan, G. M. Nikolopoulos, P. Lambropoulos, *Phys. Rev. A* **2010**, *81*, 042307.
11. A. Zwick, G. A. Álvarez, J. Stolze, O. Osenda, *Phys. Rev. A* **2011**, *84*, 022311.
12. A. Zwick, G. A. Álvarez, J. Stolze, O. Osenda, *Phys. Rev. A* **2012**, *85*, 012318.
13. S. Oh, L. Wu, Y. Shim, J. Fei, M. Friesen, X. Hu, *Phys. Rev. A* **2011**, *84*, 022330.
14. G. M. Nikolopoulos, *Phys. Rev. A* **2013**, *87*, 042311.
15. R. Ronke, T. P. Spiller, I. D'Amico, *Phys. Rev. A* **2011**, *83*, 012325.
16. Z.-M. Wang, L.-A. Wu, M. Modugno, W. Yao, B. Shao, *Sci. Rep.* **2013**, *3*, 03128.
17. M. B. Plenio, F. L. Semião, *New J. Phys.* **2005**, *7*, 73.
18. D. Burgarth, V. Giovannetti, S. Bose, *J. Phys. A: Math. Gen.* **2005**, *38*, 6793–6802.
19. D. Burgarth, V. Giovannetti, S. Bose, *Phys. Rev. A* **2007**, *75*, 062327.
20. G. Gualdi, V. Kostak, I. Marzoli, P. Tombesi, *Phys. Rev. A* **2008**, *78*, 022325.
21. E. B. Fel'dman, E. I. Kuznetsova, A. I. Zenchuk, *Phys. Rev. A* **2010**, *82*, 022332.
22. M. Murphy, S. Montangero, V. Giovannetti, T. Calarco, *Phys. Rev. A* **2010**, *82*, 022318.
23. L. Campos Venuti, S. M. Giampaolo, F. Illuminati, P. Zanardi, *Phys. Rev. A* **2007**, *76*, 052328.
24. L. Campos Venuti, C. Degli Esposti Boschi, M. Roncaglia, *Phys. Rev. Lett.* **2007**, *99*, 060401.
25. M. Christandl, N. Datta, A. Ekert, A. J. Landahl, *Phys. Rev. Lett.* **2004**, *92*, 187902.
26. M. Christandl, N. Datta, T. C. Dorlas, A. Ekert, A. Kay, A. J. Landahl, *Phys. Rev. A* **2005**, *71*, 032312.
27. A. Kay, *Phys. Rev. A* **2006**, *73*, 032306.
28. A. Kay, *Int. J. Quantum Inf.* **2010**, *08*, 641.
29. A. Wójcik, T. Łuczak, P. Kurzyński, A. Grudka, T. Gdala, M. Bednarska, *Phys. Rev. A* **2005**, *72*, 034303.
30. L. Banchi, T. J. G. Apollaro, A. Cuccoli, R. Vaia, P. Verrucchi, *Phys. Rev. A* **2010**, *82*, 052321.
31. A. Zwick, O. Osenda, *J. Phys. A: Math. Theor.* **2011**, *44*, 105302.
32. N. Y. Yao, L. Jiang, A. V. Gorshkov, Z. Gong, A. Zhai, L. Duan, M. D. Lukin, *Phys. Rev. Lett.* **2011**, *106*, 040505.
33. L. Banchi, A. Bayat, P. Verrucchi, S. Bose, *Phys. Rev. Lett.* **2011**, *106*, 140501.
34. L. Banchi, T. J. G. Apollaro, A. Cuccoli, R. Vaia, P. Verrucchi, *New J. Phys.* **2011**, *13*, 123006.
35. M. Bruderer, K. Franke, S. Ragg, W. Belzig, D. Obreschkow, *Phys. Rev. A* **2012**, *85*, 022312.
36. T. Linneweber, J. Stolze, G. Uhrig, *Int. J. Quantum Inf.* **2012**, *10*, 1250029.
37. S. Lorenzo, T. J. G. Apollaro, A. Sindona, F. Plastina, *Phys. Rev. A* **2013**, *87*, 042313.
38. W. Qin, C. Wang, G. L. Long, *Phys. Rev. A* **2013**, *87*, 012339.
39. N. Y. Yao, Z.-X. Gong, C. R. Laumann, S. D. Bennett, L.-M. Duan, M. D. Lukin, L. Jiang, A. V. Gorshkov, *Phys. Rev. A* **2013**, *87*, 022306.
40. Y. Wang, F. Shuang, H. Rabitz, *Phys. Rev. A* **2011**, *84*, 012307.
41. T. D. Ladd, F. Jelezko, R. Laflamme, Y. Nakamura, C. Monroe, J. L. O'Brien, *Nature* **2010**, *464*, 45–53.
42. J. Stolze, G. A. Álvarez, O. Osenda, A. Zwick in *Quantum State Transfer and Quantum Network Engineering*, G. M. Nikolopoulos, I. Jex (Eds.), Springer Series in Quantum Science and Technology, Springer, Berlin, **2014**.
43. M. Yung, *Phys. Rev. A* **2006**, *74*, 030303.
44. E. H. Lieb, D. W. Robinson, *Commun. Math. Phys.* **1972**, *28*, 251–257.
45. L. B. Levitin, T. Toffoli, *Phys. Rev. Lett.* **2009**, *103*, 160502.
46. E. Hamza, R. Sims, G. Stolz, *Commun. Math. Phys.* **2012**, *315*, 215–239.
47. C. K. Burrell, J. Eisert, T. J. Osborne, *Phys. Rev. A* **2009**, *80*, 052319.
48. C. K. Burrell, T. J. Osborne, *Phys. Rev. Lett.* **2007**, *99*, 167201.

Appendix A Gaussian distribution of $P_{k,1}^{lin}$

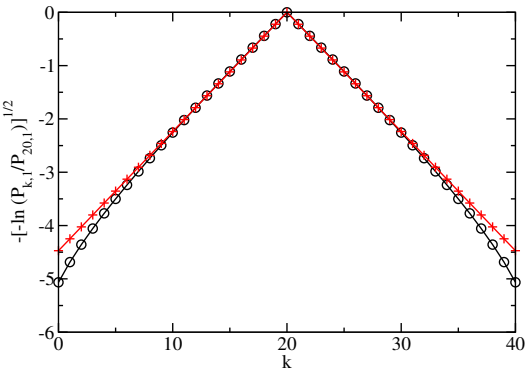

Fig. A.1 (Color online) The probabilities $P_{k,1}$ obtained using the exact expression (A.3) (black circles) and the Gaussian approximation (A.4) (red plus signs), for a 41-site chain with sites labeled $k = 0, 1, ..., 40$. Plotted is minus the square root of $-\ln(P_{k,1}/P_{20,1})$, so that the Gaussian is represented by two straight lines.

The normalized eigenstates of a chain of $N+1$ spins $1/2$ with XX-type couplings between sites l and $l+1$ given by

$$J_l = \sqrt{(l+1)(N-l)} \tag{A.1}$$

are Krawtchouk polynomials [5]. The amplitude of the ground state at site $l(= 0, 1, ..., N)$ is

$$\phi_0(l) = \sqrt{\frac{1}{2^N}\begin{pmatrix} N \\ l \end{pmatrix}}, \tag{A.2}$$

that is, the square root of the binomial distribution,

$$b(l, N, p) = \begin{pmatrix} N \\ l \end{pmatrix} p^k (1-p)^{N-k} \tag{A.3}$$

for $p = \frac{1}{2}$, with expectation value $\langle l \rangle = Np = \frac{1}{2}$ and variance $\sigma^2 = Np(1-p) = \frac{N}{4}$. For large values of N the binomial distribution approaches the Gaussian distribution (with the same expectation value and variance) in the range where the probability is non-negligible; that is,

$$|\phi_0(l)|^2 \approx \sqrt{\frac{2}{N\pi}} \exp\left(-\frac{2}{N}\left(l - \frac{N}{2}\right)^2\right). \tag{A.4}$$

Figure A.1 shows the probabilities $P_{k,1}$ calculated using the exact amplitudes, Eq. A.3, and the Gaussian approximation given by Eq. A.4, for a spin chain with $N = 40$ (that is, with 41 spins). Obviously the agreement between the exact and approximate probabilities is excellent particularly at, and near, the center of the band of eigenvalues.